

Model problems for the tear film in a blink cycle: single-equation models

R. J. BRAUN¹ AND P. E. KING-SMITH²

¹Department of Mathematical Sciences, University of Delaware, Newark, DE 19711, USA

²College of Optometry, The Ohio State University, Columbus, OH 43218-2342, USA

(Received 9 October 2006 and in revised form 29 April 2007)

We consider model problems for the tear film over multiple blink cycles in limits that yield a single equation for the tear film; the single nonlinear partial differential equation that governs the film thickness arises from lubrication theory. The two models arise from considering the absence of naturally occurring surfactant and the case when the surfactant strongly affects the surface tension. The film is considered on a sinusoidally varying domain length with specified film thickness and volume flux at each end; only one end of the domain is moving, which is analogous to the upper eyelid moving with each blink. A main contribution of this article is computation of solutions for multiple complete blink cycles; the results of these non-trivial computations show a distinct similarity to quantitative *in vivo* observations of the tear film under partial blink conditions. A transition between periodic and non-periodic solutions has been estimated and this may be a criterion for what is effectively a full blink according to fluid dynamic considerations.

1. Introduction

We create and solve a model problem for the evolution of tear film over multiple blink cycles. The blink cycle includes the upstroke of the eyelid when the tear film is formed, the open phase where the lids are fully open, and the downstroke of the eyelid where film regeneration is begun. Papers containing theoretical descriptions of the human tear film fall into three categories. The first and largest category describes evolution of the tear film during the open phase of the blink cycle; Jones *et al.* (2005, 2006) recently initiated work in the second category which treats both the upstroke and open phases of the blink cycle. To our knowledge, Braun (2006) and this paper comprise the third category in which the entire blink cycle is treated.

In this paper we study two model problems which include many essential elements of the blink cycle that forms the tear film. The tear film is assumed to be a Newtonian fluid and lubrication theory is applied to a two-dimensional model geometry for the eye. The problems incorporate two models for the deforming tear–air interface of the tear film: a clean interface (assumes a pure tear fluid) and a uniform stretching model of the interface (resulting from a strong insoluble surfactant). The equations are new because they incorporate slip at the eye surface. In this paper we present new results for complete blink cycles approximating the tear film, for the minimum blink required to completely renew the tear film and comparison with quantitative *in vivo* tear film thickness measurements; these results go well beyond those of Braun (2006). This paper is the first, to our knowledge, to compare the computed film profiles with quantitative partial blink tear film thickness measurements. We begin with a brief

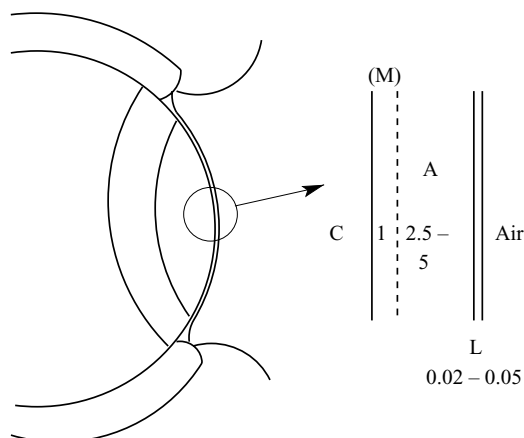


FIGURE 1. A sketch of the pre-corneal tear film. Here C denotes the cornea, M a possible mucus layer, A the aqueous layer and L the lipid layer. Typical thicknesses for are given for each layer in microns. The roles of the lipid and mucus layers will be reduced to appropriate boundary conditions for the aqueous layer. Following Berger & Corrsin (1974), the cornea is modelled as a flat wall because the tear film thickness is very small compared to the radius of curvature of the eye surface.

introduction to the tear film and then describe relevant prior theoretical treatments of it.

The human tear film has been considered to be a three-layer film that plays a number of roles in maintaining the health and function of the eye (Ehlers 1965; Mishima 1965). A sketch of the eye and the overlying tear film is shown in figure 1. Mucus is secreted from goblet cells and provides a possible first layer above the epithelial cells (Rolando & Refojo 1983; Sharma, Khanna & Reiter 1999); such a mucus layer is thought to be gel-forming mucins that are found among the bumps, or microplacae, and among long trans-membrane mucins that protrude (about $0.3\ \mu\text{m}$) from those microplacae (Gipson 2004; Bron *et al.* 2004; Chen *et al.* 1997). The surface of these mucins is modelled by a smooth surface for the purposes of fluid dynamic modelling after Braun & Fitt (2003), for example.

The aqueous layer is primarily water (about 98 %, with a variety of components forming the balance) and lies above the cornea and any possible mucus layer (Mishima 1965; Fatt & Weissman 1992); the aqueous layer is, essentially, what is commonly thought of as tears. King-Smith *et al.* (2004) point out that the interface between the aqueous and mucus layer, if there is a sharp interface, is difficult to observe experimentally and no such interface is observed *in vivo* with interferometry or other optical means; see also the discussion of the rat tear film in Chen *et al.* (1997). We note that consideration of the mucus layer as a separate entity from the other layers of the tear film is still a matter of debate which will not be settled here. In this work, we will take the tear film thickness to be in the range of 2.5 to $5\ \mu\text{m}$, consistent with *in vivo* interferometric measurements (Fogt, King-Smith & Tuell 1998; King-Smith *et al.* 2000; Nichols & King-Smith 2003; King-Smith *et al.* 2004) and optical coherence tomography (Wang *et al.* 2003).

The outermost (lipid) layer is composed of a non-polar layer above the aqueous layer with polar surfactants at the aqueous/lipid interface (McCulley & Shine 1997; Bron *et al.* 2004); it decreases the surface tension of, and the evaporation rate from,

the air/tear film interface and thus helps stabilize the tear film against rupture ('tear film break up' in the eye literature).

In this work we focus on the evolution of the aqueous layer and, based on the arguments in Braun & Fitt (2003), Zhang, Matar & Craster (2003*b*) and references therein, we assume that any mucus/aqueous interface is a flat boundary with hydrodynamic slip while the lipid layer is either ignored or modelled as a deformable, uniformly stretching surface.

We now turn to prior work on fluid dynamic theory of the tear film. In a series of papers by Tiffany and coworkers, the human tear film has been shown to be weakly shear thinning (Tiffany 1991, 1994; Pandit *et al.* 1999) and have very small elasticity (Tiffany 1994). In these papers, tear fluid was extracted from the eye and then its viscosity and storage modulus measured for different shear rates using a commercial viscometer. Some differences in the shear thinning was observed between normal tears and those from marginally dry eye patients (Tiffany 1991), and how to incorporate this information about the tear film is a significant question. Computations for slot coating with viscoelastic fluids, which are driven thin films, typically show little effect on the surface shape, but may have dramatically altered stress profiles in the fluid (Lee, Shaqfeh & Khomami 2002; Pasquali & Scriven 2002). Perturbation approaches to thin film problems can certainly show some differences (Zhang, Matar & Craster 2003*a*; Myers 2005) and including general effects in a perturbation approach must be handled with some care due to the presence of steep gradients in the stress fields over a very wide range of parameter space (Beris *et al.* 1983; Zhang & Li 2005). We consider only a Newtonian film and non-Newtonian effects are beyond the scope of this paper.

Theoretical studies of the pre-corneal tear film in the open phase include Braun & Fitt (2003), Wong, Fatt & Radke (1996), Sharma *et al.* (1998) and Miller, Polse & Radke (2003); all of these have used Newtonian film properties but Wong *et al.* (1996) were the first to use the tangentially immobile approximation for the tear film surface. All of these studies found that reasonable times to rupture were possible in various lubrication models for the thin film evolution and all found t^α thinning, with $\alpha = -0.45$ or -0.46 , of the thinnest point in the film (located near the menisci). Korb & Herman (1979) show that this 'black line' region near the meniscus can give rise to corneal staining that is presumably due to film rupture and subsequent epithelial damage. Braun & Fitt (2003) and Wong *et al.* (1996) used standard lubrication theory; Sharma *et al.* (1998) kept the full curvature term from the normal stress condition on the tear film surface in an effort to incorporate the meniscus in an improved fashion. Miller *et al.* (2003) also kept the full curvature of the tear film surface, but the boundary condition that was intended to be a no-flux condition in that paper is inconsistent with their evolution equation for the film; the overall conclusions are expected to be roughly correct however.

Braun & Fitt (2003) added gravitational and evaporative effects. Gravity was shown to contribute to Newtonian tear film evolution if the film is assumed to have a typical thickness of 10 μm . Under those conditions, gravity breaks symmetry between the upper and lower menisci and adds a bias for the tear film to break up (rupture) in the upper part of the tear film due to decreased film thickness there. Gravity typically makes a small contribution for normal interblink times on the order of 5 s and for the smaller, more recently measured tear film thicknesses of about 3 μm (King-Smith *et al.* 2004; Wang *et al.* 2003). In Braun & Fitt (2003), it was also shown that evaporation could combine with capillary-driven thinning to accelerate tear film breakup. The effect was greater than would be expected due to evaporation alone

because the evaporative thinning and capillary-driven thinning cooperated so that evaporation was important late in the thinning process near the menisci.

The formation of the tear film was studied as a coating problem first by Wong *et al.* (1996), using a quasi-steady analysis that modified the Landau–Levich dip coating problem (Levich 1962; Probstein 1994); both drainage and formation were studied. They predicted a reasonable range of thicknesses in the micron range from their theory; Creech *et al.* (1998) used the approach to derive tear film thicknesses from meniscus radius measurements and tear film thicknesses from 2.4 to 24 μm were estimated. More recent work analysing the tear film volume suggests that this theory may be insufficient to spread the tear film without a supply of tear film from under the lids (King-Smith *et al.* 2004).

Models for tear film were significantly advanced by Jones *et al.* (2005); they developed a lubrication model that allowed the combined study of film formation during the eyelid upstroke and the evolution during the open phase. Their model did not include the downstroke and so did not compute a complete blink cycle. They also incorporated model fluxes to approximate tear supply from beneath the moving upper eyelid. They found that no-flux conditions did not allow sufficient coverage of the underlying surface and that a flux of tear fluid from the eyelids was needed to provide adequate coverage; this conclusion supported the analysis based on available tear volume by King-Smith *et al.* (2004). They also verified that, in most cases, the piecewise parabolic initial conditions often used in previous tear film drainage calculations during the open phase produced results quite similar to those where the film was generated from an upstroke and then allowed to evolve.

Braun (2006) began studying the blink cycle theoretically by using sinusoidal lid motion and with sinusoidal fluxes through the ends. Using that simplified blink model, he found solutions for multiple blink cycles using both full and partial blink cycles. The model motion and flux functions are chosen as an initial step toward incorporating the theory of the lacrimal drainage system due to Doane (1981) for the blink cycle in the thin film evolution on the eye surface. In Doane's theory, each blink cycle has a period at the end of the upstroke and beginning of the open phase in which tear fluid may be extracted from the tear film and drained down the canaliculi (Doane 1981); the theories of Jones and coworkers have not taken this aspect of the tear film into account. Periodic solutions for the film were observed for 'full' blink cycles while this aspect of the evolution is lost for partial blinks; the transition between these two behaviours reveals a minimum blink required to completely 'reset' the tear film.

While this work was being concluded, Jones *et al.* (2006) further advanced tear film modelling by developing a model of the tear film with a mobile surface and a model insoluble surfactant. They calibrated their model with experimental observation of particle motions from Owens & Phillips (2001). They found thin regions of tear fluid that propagated superiorly (toward the upper lid) following the upstroke which began from a partly open position. This behaviour was also observed using fluorescein dye *in vivo*, but the observations are limited to a qualitative nature.

In this work, we continue to study the simplified tear film with sinusoidal lid motion and fluxes. A more complete exploration of the model behaviour is given in comparison to Braun (2006); this includes results for the dependence of the transition between periodic and non-periodic solutions on the tear film volume. A mathematical derivation of the uniform stretching limit (the strong surfactant case) is also given here. We find an encouraging comparison between partial blink modelling

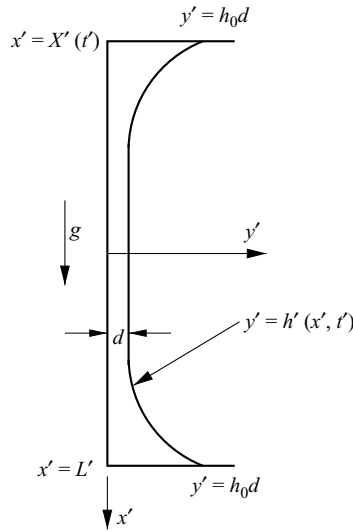


FIGURE 2. A sketch of the pre-corneal tear film indicating important mathematical quantities. The dimensional upper lid location is $X'(t)$; this end moves in blink cycle models.

as carried out here with *in vivo* measurement of the pre-lens tear film thickness which is quantitative.

We begin with the problem formulation in the next section, then present results in §3, followed by discussion and conclusions in subsequent sections.

2. Formulation

A sketch of the mathematical model for the tear film is shown in figure 2. The coordinate directions (x, y) and velocity components (u, v) are along and perpendicular to the flat surface that approximates the corneal surface. The scalings are as follows. $L' = 5\text{ mm}$ is half the width of the palpebral fissure and is taken in the x -direction; the characteristic thickness of the tear film away from the ends is $d = 5\text{ }\mu\text{m}$. The ratio of the length scales, $\epsilon = d/L'$, is the small parameter for lubrication theory; for the above scales, $\epsilon \approx 10^{-3}$. The velocity scale along the film is the maximum or mean blink closing speed, $U_m = 10\text{--}30\text{ cm s}^{-1}$ for the maximum speed case (Doane 1980; Berke & Mueller 1998); however, we will not be able to achieve this parameter range with our current numerical method. ϵU_m is the characteristic speed across the film. The time scale is $L'/U_m = 0.05\text{ s}$ for real blink speeds. We will use the following properties: the surface tension $\sigma_0 = 45\text{ mN m}^{-1}$, the density $\rho = 10^3\text{ kg m}^{-3}$, the viscosity $\mu = 10^{-3}\text{ Pa s}$ and $g = 9.81\text{ m s}^{-2}$. The subscript 0 indicates evaluation at a reference value; in this case, we view it as the fully open state with lowest average surface concentration as this value was measured from open eyes. The pressure p is made non-dimensional with the viscous scale $\mu U_m/(d\epsilon)$.

Non-dimensionalization results in the following leading-order parallel flow problem on $0 \leq y \leq h(x, t)$:

$$u_x + v_y = 0, \quad u_{yy} - p_x + G = 0, \quad p_y = 0. \tag{2.1}$$

The equations are for mass conservation, and momentum conservation in the x and y directions, respectively. The inertial terms in the x -component of momentum conservation are proportional to ϵRe where $Re = \rho U_m d/\mu$ is the Reynolds number;

using the small value of U_m , $Re \approx 1$, but the factor ϵRe is small and we neglect it. The inertial terms in the other momentum equation are proportional to $\epsilon^3 Re$ and the viscous terms are $O(\epsilon^2)$ or smaller. Here

$$G = \frac{\rho g d^2}{\mu U_m} \quad (2.2)$$

is the Stokes number. For typical blink conditions and normal tear film thicknesses, $G \approx 2.5 \times 10^{-3}$. The small Stokes number means that computations will have to continue for long times to see any significant effect of gravity; results of Jones *et al.* (2005) illustrated this and we will neglect it in this paper.

On the impermeable wall at $y=0$ the boundary conditions are

$$u = \beta u_y, \quad v = 0; \quad (2.3)$$

the first condition is the Navier slip condition and the second is impermeability. Here $\beta = L_s/d$ is the slip coefficient where L_s is the slip length; this parameter was discussed in Braun & Fitt (2003) and was expected to be in the range $10^{-3} \leq \beta \leq 10^{-2}$. One may also argue that L_s is based on a molecular length scale, and perhaps the largest size is that of membrane-bound mucins at about $0.3 \mu\text{m}$; using this scale gives $\beta \approx 10^{-1}$ but this is probably too large for the tear fluid. Using the size of water molecules gives a much smaller β but this ignores any mucin effect. The slip condition is required to relieve a stress singularity at the junction of the lid with the eye surface if the eyelid is assumed to act as a ‘windshield wiper,’ while opening and closing, similar to the problem with a moving contact line. The case can be made that there is a fluid film under the moving lid that prevents a singularity from the putative surface of the cornea (Jones *et al.* 2005; Huh & Scriven 1971), but there still may be slip at the surface of the eye (Zhang *et al.* 2003*b*) due to the complex surface there (Gipson 2004; Bron *et al.* 2004). We assume that values of slip at the corneal surface are near the large end of the available range as indicated above, in alignment with these authors, and we choose to include slip in an attempt to model this surface more closely and we choose $\beta = 10^{-2}$ in all cases. We do not include any intermolecular or van der Waals forces here; they will be treated in a future paper.

At the free surface, we have the kinematic and stress conditions

$$h_t + u h_x = v, \quad p = -S h_{xx}, \quad u_y = M \Gamma_x, \quad (2.4)$$

where

$$S = \frac{\epsilon^3}{Ca} = \frac{\epsilon^3 \sigma}{\mu U_m}, \quad M = \left(\Gamma \frac{\partial \sigma}{\partial \Gamma} \right)_0 \frac{\epsilon}{\mu U} = \frac{\hat{M}}{\epsilon}. \quad (2.5)$$

Here $Ca = \mu U_m / \sigma_0$; for the lowest maximum speed, we find $Ca \approx 2 \times 10^{-3}$ and $S \approx 5 \times 10^{-7}$; such small values will not be accessible and we will discuss this further. $\Gamma = \Gamma(x, h, t)$ is the surface concentration of a polar component of the lipid layer at the lipid–aqueous surface; this is what we mean by the surfactant on the free surface. We estimate that $(\Gamma \partial \sigma / \partial \Gamma)_0 = 0.01 \text{ N m}^{-1}$, and using real blink parameters, we estimate $\hat{M} = 10^{-4}$ and $M = 0.1$. This is a significant value for the Marangoni effect that is plausible in comparison with ocular surface observations (Berger & Corrsin 1974; Owens & Phillips 2001). The surface concentration of a polar component of the lipid layer at the lipid–aqueous interface is governed by the transport equation

$$\Gamma_t + (u^{(s)} \Gamma)_x = P^{-1} \Gamma_{xx}. \quad (2.6)$$

Here $u^{(s)}$ is the surface velocity, $P^{-1} = D/L'U$ is the Péclet number and D is the surface diffusivity of Γ . With $D = 10^{-9}\text{m}^2\text{s}^{-1}$, we estimate $P^{-1} \approx 2 \times 10^{-6}$; diffusion of surfactant is small during the blink itself and the surface diffusion term is neglected.

The two cases of this paper differ in the treatment of the tangential stress boundary condition. In §2.1, the film is treated as a pure liquid with a clean surface in contact with a passive gas. In §2.2, the pure fluid has an insoluble surfactant at its interface with the passive gas, and the effect on the surface tension is so strong that the surface responds in a manner that is analogous to the tangentially immobile case when the domain length is fixed. Jones *et al.* (2005) called these limits the inactive and active lipid layers, respectively; we shall use the terms stress-free and uniform stretching.

In either case, the flux is given by

$$Q = \int_0^h u(x, y, t) dy, \tag{2.7}$$

then, using the kinematic condition and mass conservation, the free surface evolution is given by

$$h_t + Q_x = 0. \tag{2.8}$$

The small capillary number means that there will be localized regions on the order of $S^{1/3}$ in width that will occur in the opening part of the cycle. We study the result from typical lubrication-type models, and we will retain the average surface tension in S and its variation via limiting cases of M as well as slip β in order to investigate the effect of the moving film end.

2.1. Stress-free free surface

If we now consider solving (2.1) subject to (2.3) and the stress-free boundary condition

$$u_y(x, h(x, t), t) = 0, \tag{2.9}$$

we find

$$u = (-p_x + G)h(y + \beta) - (-p_x + G)\frac{y^2}{2} \tag{2.10}$$

and

$$Q = (-p_x + G) \left(\frac{h^3}{3} + \beta h^2 \right). \tag{2.11}$$

Substitution into (2.8) yields a standard evolution for $h(x, t)$ that can be found in Oron, Davis & Bankoff (1997) for example.

2.2. Large- M limit

When the Marangoni effect is very strong, there is another simplification to a single equation. This uniform-stretching limit was first proposed by Jones *et al.* (2005) to our knowledge, but they did not give a derivation of this limit and we give one here. The tangential stress condition requires $\Gamma_x = 0$ on the free surface in this limit. The surfactant transport equation becomes

$$\Gamma_t + u_x^{(s)}\Gamma = 0. \tag{2.12}$$

Because the concentration is spatially uniform but still time-varying, we may write

$$\Gamma = \frac{2L}{L - X(t)}\Gamma_m, \quad \frac{d\Gamma}{dt} = \frac{2L}{(L - X(t))^2}X_t\Gamma_m. \tag{2.13}$$

Here Γ_m is a constant and is the minimum concentration during the cycle (fully extended domain). Substitution into the surfactant transport equation gives

$$u_x^{(s)} = -\frac{X_t}{L-X}; \quad (2.14)$$

solving the ODE for $u^{(s)}$ and using $u^{(s)}(L, t) = 0$ gives

$$u^{(s)} = X_t \frac{L-x}{L-X}. \quad (2.15)$$

Computing the flux yields

$$Q(x, t) = \frac{h^3}{12} \left(1 + \frac{3\beta}{h+\beta}\right) (Sh_{xxx} + G) + X_t \frac{L-x}{L-X} \frac{h}{2} \left(1 + \frac{\beta}{h+\beta}\right) \quad (2.16)$$

and substituting into (2.8) yields the single PDE for $h(x, t)$ in this case. Note that if $X_t = 0$, we recover the equation for the free surface with slip on the bottom surface but a tangentially immobile ($M \gg 1$) free surface. If $\beta = 0$ as well, we recover the tangentially immobile case with a no-slip bottom surface.

2.3. Film ends: lid motion and boundary conditions

The film is contained in the interval $X(t) \leq x \leq L$. At the right-hand end of the domain, $x = L$ and this boundary location will be fixed for all time. At the left-hand end, $x = X(t)$, we apply the same kinds of boundary conditions; when $X = -L$, the film is fully open. $L = 1$ in this paper.

At the ends of the film, we have a specified film thickness and volume flux. In Bron *et al.* (2004) and references therein, the tear film is thought to remain pinned in the neighbourhood of the exits from the meibomian glands; this is our motivation for fixing the film thickness. We note that there may be other possible boundary conditions, particularly under extreme conditions, but they are beyond the scope of this paper. The film thickness is pinned at $h_0 = 13$ at the ends for all cases in this paper.

A mathematical fit to the lid position at the centre of the palpebral fissure was obtained by Berke & Mueller (1998) for the data in Berke & Mueller (1996); comparison was made with similar data of Doane (1980). Blink data were also measured and fit by Jones *et al.* (2005); they only computed solutions for the upstroke of the eyelid and subsequent open time. Here, the upper lid position is given by

$$X(t) = L[(1-\lambda)\cos(t) - \lambda]; \quad (2.17)$$

λ is the fraction of the fully open region that is still open when the domain is at its smallest. We shall consider $\lambda = 0.1$ as fully closed for the purposes of this paper. With $\lambda = 0.5$, the domain half closes during the blink cycle. This is simpler than the measurements and fits that appear in the literature for the complete blink cycle, but we consider sinusoidal motion in order to understand a fundamental case of a complete blink cycle for later comparison with measured motions (Heryudono *et al.* 2007).

We study only sinusoidal fluxes from the tear film ends. These fluxes model the flow along the lids during the blink cycle as described by Doane (1981). We note that there are limitations to using sinusoidal flux functions, but we are satisfied that they are adequate to begin understanding this model system. We use the non-dimensional flux functions

$$Q_{top} = Q_{mT} + Q_{OT} \sin(t + \phi) \quad \text{at } x = X(t), \quad (2.18)$$

$$Q_{bot} = Q_{mT} [\sin(t + \phi) - 1], \quad \text{at } x = L. \quad (2.19)$$

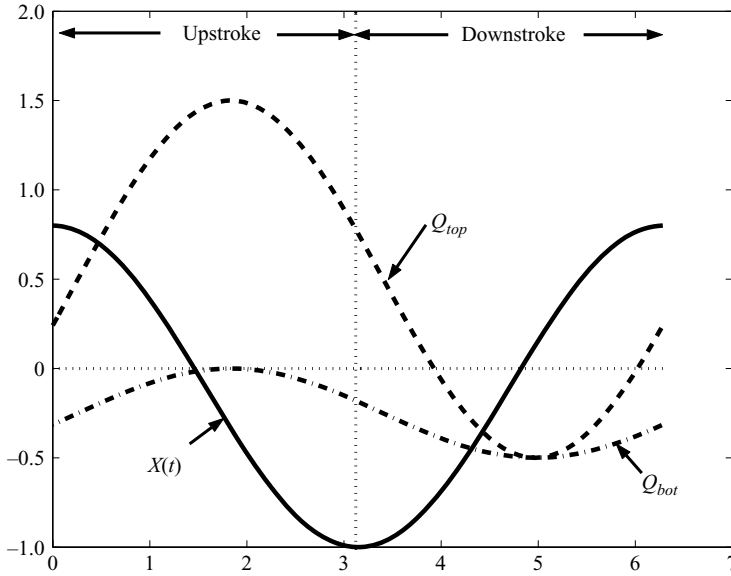


FIGURE 3. An example of the lid motion $X(t)$ and boundary fluxes Q_{bot} and Q_{top} for $\lambda = 0.1$, $Q_{mT} = 0.5$, $Q_{0T} = 1$ and $\psi = \pi/4$. The domain is fully open at $t = \pi$ with $X = -1$ and fully closed at $t = 0, 2\pi$ with $X = 1 - 2\lambda$. The upstroke (opening phase of the blink) is from $0 < t < \pi$ and the downstroke (closing phase) is from $\pi < t < 2\pi$. Note that Q_{top} becomes negative after the domain is fully open.

The choice for Q_{bot} ensures that the tear film volume is conserved over a blink cycle of duration 2π . The mean value of the volume flux in at the top, Q_{mT} , and the amplitude of the oscillation of the flux, Q_{0T} for the zero-mean part, are specified as input parameters. The mean level of flow from the lacrimal gland has been estimated to be about $1.2 \mu\text{l min}^{-1}$ (Mishima 1965); non-dimensionalizing this flux with $U_m dL$ gives $Q_{mT} = 0.01$, which assumes that the influx of new tears is spread out uniformly along the upper eyelid. We study flux values on this order, which we believe is reasonable given the assumed motion of the ends.

Typically, the phase offset from the lid location, $\phi = \phi_0$, is computed so that outflux at the top begins when the domain is at its largest; this requires, after enforcing $Q_{top}(\pi) = 0$ and some trigonometric manipulation,

$$\phi_0 = \sin^{-1}(Q_{mT}/Q_{0T}). \tag{2.20}$$

Note that the amplitude of the oscillation Q_{0T} must be at least as large as the mean value Q_{mT} in order for ϕ_0 to exist. We will also examine more general phase shifts

$$\phi = \phi_0 - \psi. \tag{2.21}$$

An example is shown in figure 3 with $\psi > 0$; note that the beginning of the outward flux from the top end ($x = X(t)$ or $\xi = -1$) begins after the domain is longest ($X(\pi) = -1$). Finally, the fluxes at each end were chosen to be in phase with each other due to the expected simultaneous opening of the canaliculi in the blink process in eyes (Doane 1981). The addition of an outflux from the ends is a new component of the modelling which was not present in that of Jones *et al.* (2005) and it represents a step toward constructing models which employ the Doane (1981) blink cycle model.

2.4. Initial condition

For the purposes of numerical solution, we find it convenient to transform the domain $X(t) \leq x \leq L$ to a fixed domain $-1 \leq \xi \leq 1$ via

$$\xi = 1 - 2 \frac{L - x}{L - X(t)}. \quad (2.22)$$

(Details are in the Appendix.) Using the change of variable $h(x, t) = H(\xi(t), t)$, the initial condition is most easily specified in terms of these new variables. We use the polynomial initial condition

$$h(x, 0) = H_{\min} + (h_0 - H_{\min})\xi^m; \quad (2.23)$$

this initial shape is applied when the domain is at its shortest, and the computation starts from this ‘closed’ state. Values from $m = 4$ to 16 were used. H_{\min} was chosen to achieve the desired volume; $h_0 = 13$ as mentioned above.

We considered two initial volumes (areas) $V_0 = 1.576$ and $V_0 = 2.576$. The latter comes from estimating the volume for a $d = 5\mu\text{m}$ film with quadratic menisci having width 0.36mm and height h_0d at both ends. The former is a lower volume that simulates a reduced tear volume from a $2.5\mu\text{m}$ film with the film ends the same height as the other case.

3. Results

3.1. Numerical method

A uniformly spaced mesh in x was used. Centred second-order-accurate finite difference approximations were used for the derivatives in a conservative form for the PDE; the same spatial discretization was used in Braun & Fitt (2003). Non-centred differences were used at the ends where appropriate. The resulting ODEs are solved using DASPK (Brenan, Campbell & Petzold 1996) in order to facilitate generalization to differential-algebraic equations if needed. To obtain sufficient accuracy as measured by conservation of volume to within 0.5% with no-flux end conditions, 4095 interior grid points were used. This was found to be the maximum number of points that could reliably be used with this approach.

Our numerical method is unable to reach the parameter range in S described above; we will investigate the range $10^{-3} \leq S \leq 2 \times 10^{-5}$ in this work, corresponding to slower end motion than actual blinks. However, a transition in behaviour occurs within this regime that we believe makes this range relevant.

3.2. Stress-free surface

Results for the full blink and no flux through the ends are shown in figure 4. In this case, $\lambda = 0.1$ and so only 10% of the film length is left then the film is closed. The entire film thickness at several times is shown in figure 4(a). This thickness is low for real tear films, but is useful for studying the behaviour in lubrication theory. In this case, $S = 10^{-4}$, which is too large for eyes but is an intermediate value for the computational range that we can access. The results show that the film does not rupture in this case; this is more clearly seen in figure 4(b), a close-up in the y -direction. The film shape repeats past $t = 2\pi$, beginning with that film shape, and we believe this has two causes because of two things. One is that the underlying flow is slow viscous flow according to the Stokes equations, whose results are known to be reversible. The second is that when the lids are fully closed, the film has essentially been entirely swept up into a small region and then respread over the substrate; this

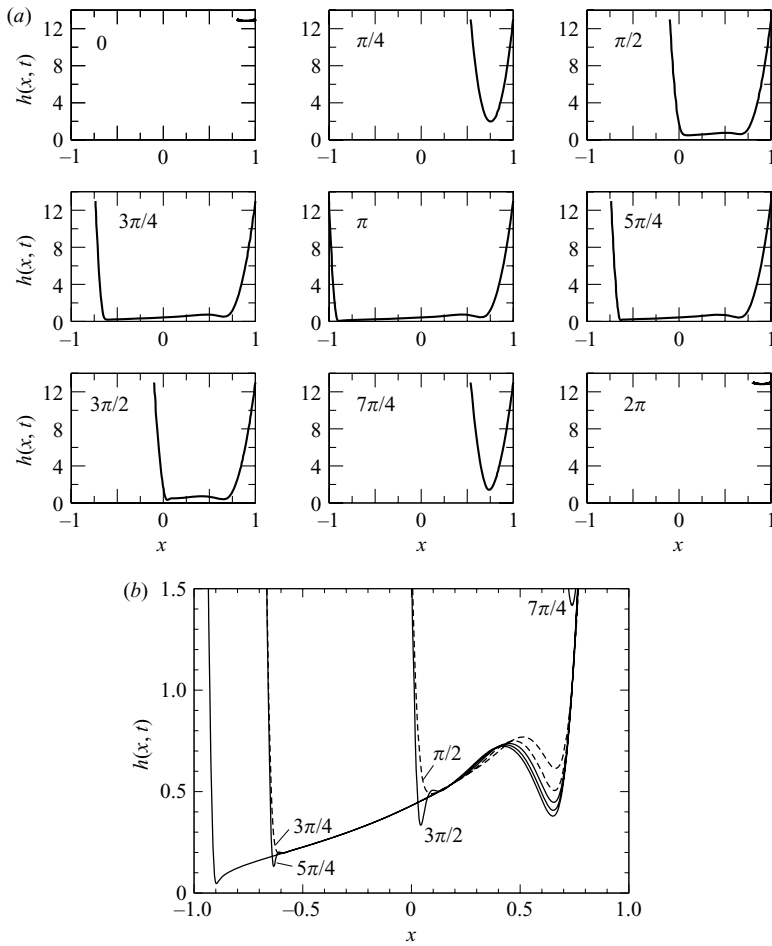


FIGURE 4. Film thickness with $S = 10^{-4}$, $\lambda = 0.1$, $m = 4$, zero boundary fluxes at the ends of the film and $V_0 = 2.576$. (a) Various times during a complete blink cycle, as indicated in each panel. (b) A close-up in the vertical direction of the same results.

is a favourable situation because relatively slow relaxation of the film shape caused by surface tension is completely erased by each blink.

Note that in these film shapes, the minimum value is sometimes at the right-hand end of the film and sometimes the left; while the film shapes as a function of x are smooth and well behaved, plotting the minimum film thickness as a function of time develops jumps in the slope. Figure 5 shows the time dependence of the minimum film thickness for the no-flux boundary conditions, $\lambda = 0.1$ and several values of S , the surface tension number, for $0 \leq t \leq 4\pi$ (two periods of end motion). The steep downward spikes are due to the minimum near the moving end and the rounded tops are for the times near full closure; the less steep parts between are from the right-hand end. The curves are complicated but periodic.

For the non-zero boundary fluxes given by $Q_{mT} = 0.04$ and $Q_{0T} = 0.08$ and $\lambda = 0.1$, periodicity remains. Plots of $h_{\min}(t)$ in figure 6 with and without the boundary flux confirm this. The plots also show that the minimum film thickness is increased when these boundary fluxes are added.

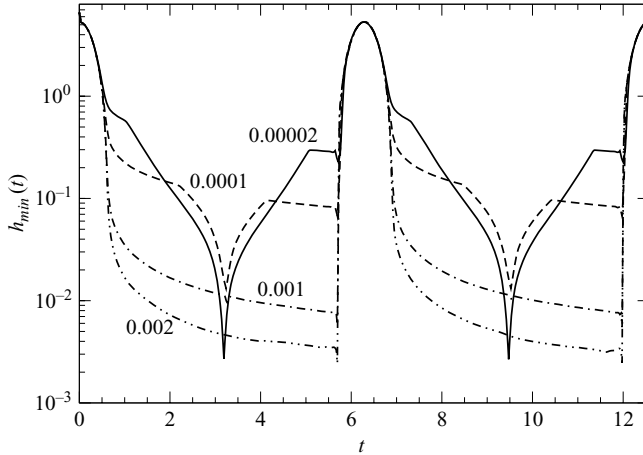


FIGURE 5. Minimum film thickness as function of time with $\lambda = 0.1$, $m = 4$, $V_0 = 1.576$, and no-flux boundaries ($Q_{mT} = Q_{0T} = 0$) at the ends of the film; results for several S are shown. The sudden changes in slope occur when the minimum film location switches ends of the film. The curves are periodic provided λ is sufficiently small.

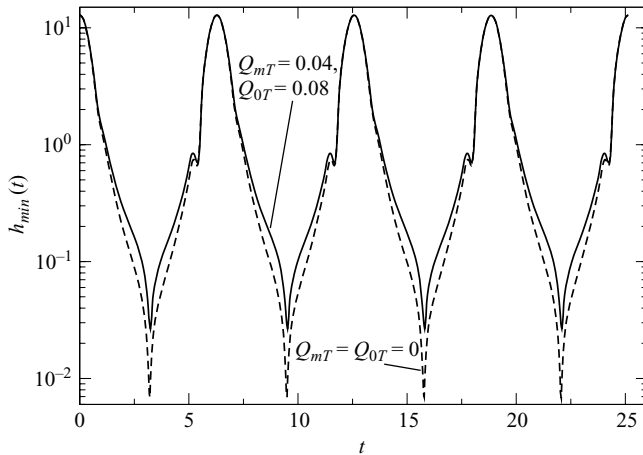


FIGURE 6. Minimum film thickness as function of time with $\lambda = 0.1$, $V_0 = 2.576$, $m = 8$ and different boundary fluxes. At t values that are odd multiples of π , the minimum film thickness is larger in the case with non-zero flux.

Results for a half-blink case are shown in figure 7; here the flux at both ends is zero. On the left half of the plot, we see a coating flow that leaves behind a tapering film. This half repeats to graphical accuracy; on the right half, slow capillary-driven motion is occurring, particularly near the right-hand boundary. Where the end sweeps the domain, the film is ‘reset’ and the film preserved; otherwise, without flux from the boundary, capillarity slowly thins the right-hand end of the film. The slow capillary thinning is reminiscent of black line formation in eyes, as has been discussed by a number of authors (Wong *et al.* 1996; Sharma *et al.* 1998; Braun & Fitt 2003; Miller *et al.* 2003; Jones *et al.* 2005).

The effect of the initial condition is shown in figure 8. Increasing the exponent m causes a higher, flatter middle region in the initial shape for the smaller volume case;

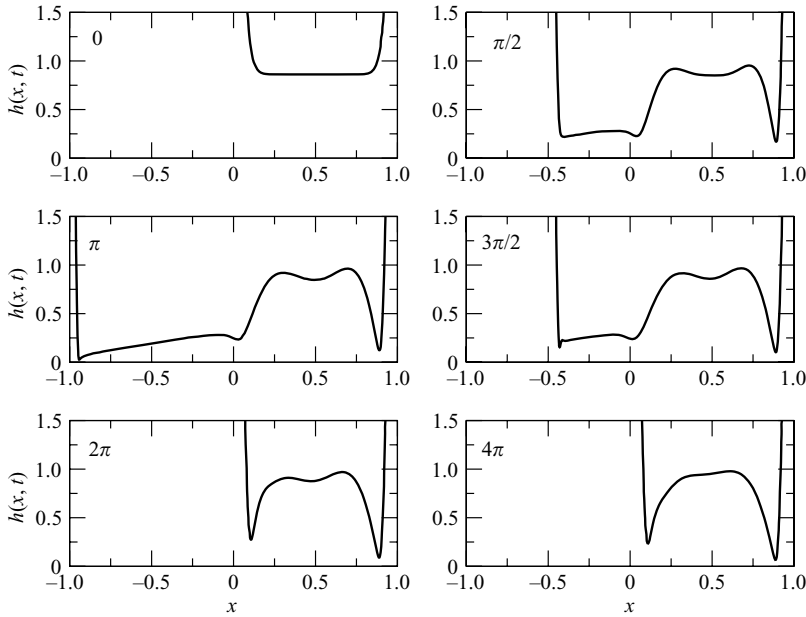


FIGURE 7. Film thickness $h(x, t)$ at various times with $\lambda = 0.5$, $S = 2 \times 10^{-5}$, $m = 16$, $V_0 = 1.576$ and $Q_{mT} = Q_{0T} = 0$ at the ends of the film. A plateau region develops in the right half of the film and persists. For the times when the domain is fully open, the small valley in the middle of the film is reminiscent of experimentally measured profiles. The bottom two panels illustrate capillary-driven relaxation; the solution is not periodic.

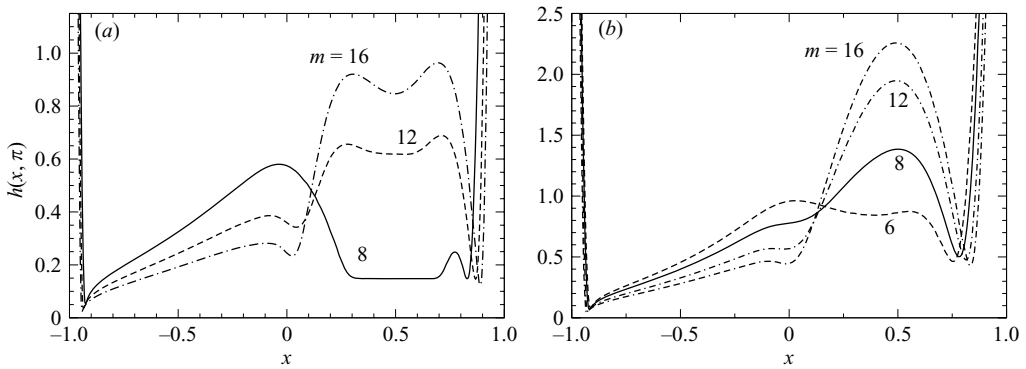


FIGURE 8. The initial condition has a significant effect on the film thickness, shown at $t = \pi$ in each case, under partial blink conditions, $\lambda = 0.5$, $S = 2 \times 10^{-5}$, $Q_{mT} = Q_{0T} = 0$. (a) $V_0 = 1.576$; (b) $V_0 = 2.576$.

the incomplete sweeping action and relatively low value of S then cause this feature to persist, resulting in the plateau on the right for larger m . For the larger volume case (figure 8b), the initial minimum film thickness is significantly larger and so the plateau region relaxes more rapidly from capillarity.

The minimum film thickness, for $\lambda = 0.5$, no-flux boundary conditions and several values of S , is shown in figure 9. In this case, the slow downward curve corresponds to the local minimum near the right-hand end of the film ($x = 1$) and the sudden downward spikes are from the blink motion causing a local minimum near the

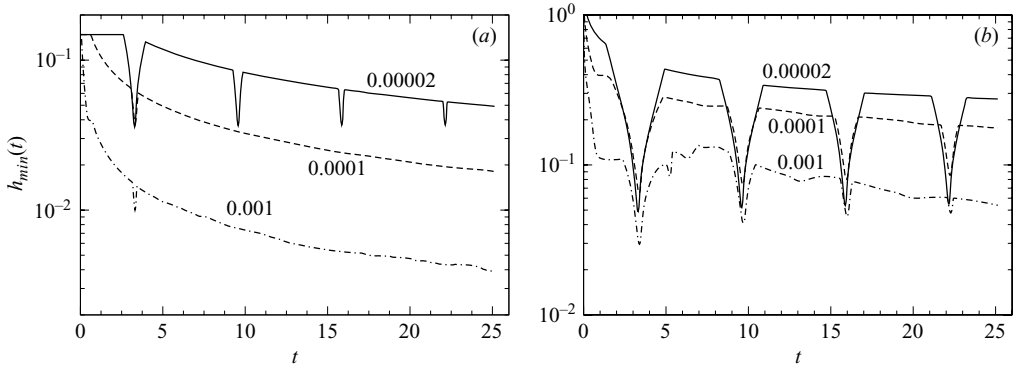


FIGURE 9. Minimum film thickness as function of time with $\lambda = 0.5$, $m = 8$ and zero boundary fluxes ($Q_{mT} = Q_{oT} = 0$) at the ends of the film: (a) $V_0 = 1.576$ and (b) $V_0 = 2.576$. Results for several S are shown. The sudden changes in slope occur when the minimum film location switches ends of the film. The function is no longer periodic for this large λ .

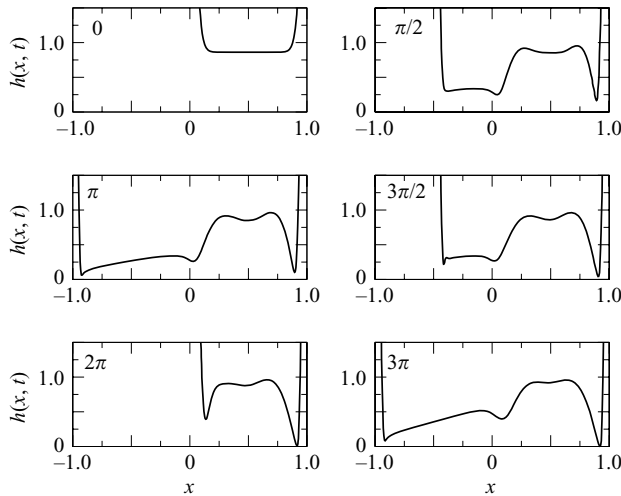


FIGURE 10. Film thickness at various times with $\lambda = 0.5$, $V_0 = 1.576$, $Q_{mT} = 0.02$, and $Q_{oT} = 0.04$. A buildup of film thickness appears to the left of the plateau when the film is fully extended at $t = 3\pi$; compare the panels at π and 3π . Fluid supplied from the moving end does not flow across the entire film length.

left-hand end of the film ($x = -1$). The case with larger film area retains the rapidly decreasing minimum from the moving end at larger values S , while the other does not. For $S > 10^{-3}$, the results are not reliable at longer times because the film thickness approaches the size of the grid step.

When there is flux through the ends of the film and a half-blink occurs, there is significant change; results are shown in figures 10 to 12. In figure 10, a buildup of film thickness appears to the left of the plateau when the film is fully extended. This occurs because the flux supplied from the moving end does not flow across the film; the slowly relaxing right-hand side of the film acts as a barrier for this newly supplied fluid. At the right-hand (fixed) end, there is a net outflow of tear fluid and this causes breakup of the film. The film appeared to touch down just after $t = 4\pi$ according to the computation; we believe that the computation loses accuracy once the film

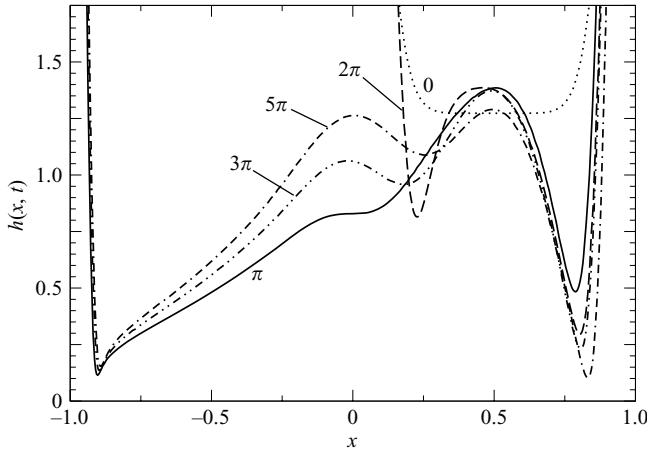


FIGURE 11. Film thickness at various times with $\lambda = 0.5$, $S = 2 \times 10^{-5}$, $m = 8$, $V_0 = 2.576$, $Q_{mT} = 0.02$, and $Q_{0T} = 0.04$. A buildup of film thickness appears in the middle of the film. The plateau on the right-hand side of the film when there is less fluid does not remain in this case because the thicker film relaxes more quickly.

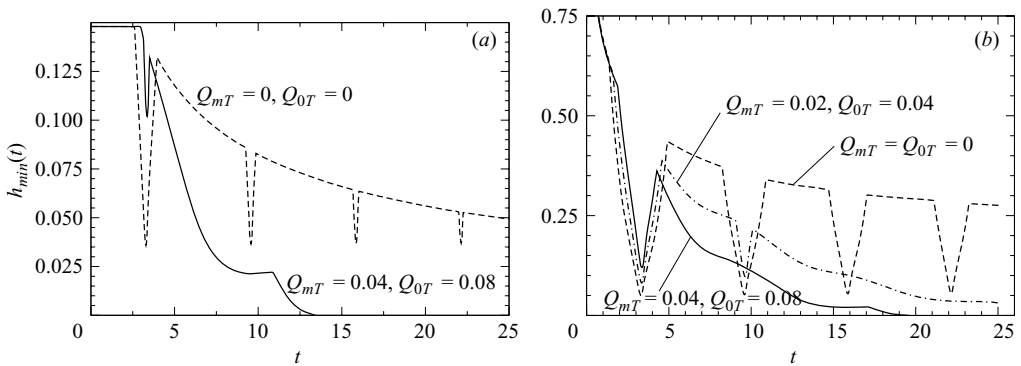


FIGURE 12. Minimum film thickness with time for $m = 8$, $S = 2 \times 10^{-5}$, $\lambda = 0.5$, and different boundary fluxes. (a) $V_0 = 1.576$; (b) $V_0 = 2.576$. At about $t = \pi$, the minimum film thickness (left-hand end) is larger in the case with non-zero flux. The right-hand end is thinned by the flux and appears to rupture with repeated half blinks in this model.

thickness reaches the mesh size and so we cannot resolve this part of the evolution. When more liquid is present in the film, as for $V_0 = 2.576$, the plateau that was in the right half of the film relaxes more rapidly than in the dryer case; figure 11 shows this case. A bump still forms in the middle of the film because the supplied fluid does not move across the film in time.

Also, the minimum thickness is significantly increased near the moving lid but decreased at the other (right-hand) end; this is most easily seen in figure 12. The smooth, curving portions of the curve correspond to the right-hand end of the film, which is steadily being drained. The single relatively sudden change comes from the motion of the left-hand end of the film and it is significantly higher than its no-flux counterpart (at about $t = \pi$). Each succeeding sudden decrease in the minimum film thickness is less deep than the previous one, due to the influx from the moving boundary. The increase of the minimum film thickness left behind at the moving

Q_{mT}	Q_{0T}	λ	
		$V_0 = 1.576$	$V_0 = 2.576$
0	0	0.178	0.211
0.01	0.02	0.154	0.193
0.02	0.04	0.147	0.187
0.04	0.08	0.142	0.185

TABLE 1. The beginning of non-periodic behaviour is estimated for the given values of λ at various boundary flux conditions with $S = 2 \times 10^{-5}$ and $h_0 = 13$. These results are for the $M = 0$ or stress-free case. We believe that these estimates are accurate to within ± 0.002 .

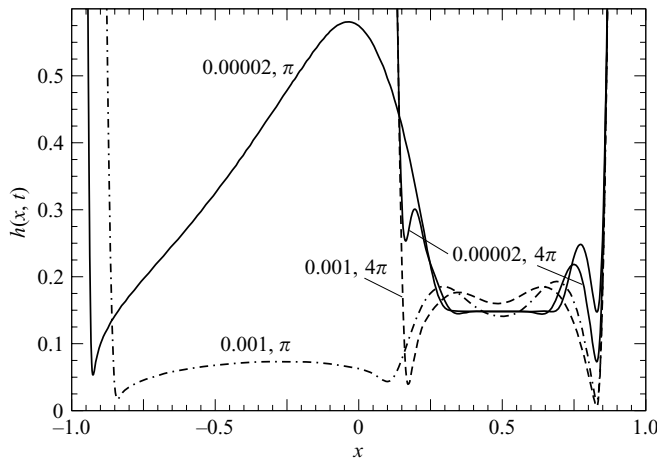


FIGURE 13. Film thickness at various times and S values with $\lambda = 0.5$, $m = 8$ and no-flux boundaries ($Q_{mT} = Q_{0T} = 0$). A bump appears in the middle of the film for the smaller value of S . The bump is enhanced with time when non-zero flux conditions are used (not shown). The larger value of S appears to retain more fluid in the menisci.

boundary with an influx of tear fluid from the upper lid agrees with the results of Jones *et al.* (2005) for the coating part of the cycle that they studied.

There is also a transition in behaviour in the surface tension number S for the smaller volume case we considered. Figure 13 shows results for the film thickness at two different times and two different values of S with no-flux conditions at the ends during half-blink cycles. The film thickness at the fully open state ($t = \pi$), shows the bump when $S = 2 \times 10^{-5}$, but the bump is absent when $S = 10^{-3}$. This suggests that there is a transition from the absence of the bump when surface tension effects are large enough to the presence of the bump when surface tension effects are weak enough. Note also the enhanced thinning and black line formation at the right-hand end when $S = 10^{-3}$. For the larger volume case, there was no transition like this for the range of S that we considered.

The different behaviours at different λ suggest that there is a transition in the behaviour of the film shapes. Using plots of $h_{\min}(t)$ and closely inspecting these curves allows us to estimate the λ at which the solution becomes periodic for decreasing λ . Results are shown in table 1; the estimates are given to 3 significant digits and it would be difficult for our numerical method to determine these values any better. Introducing flux through the upper and lower boundaries requires a smaller

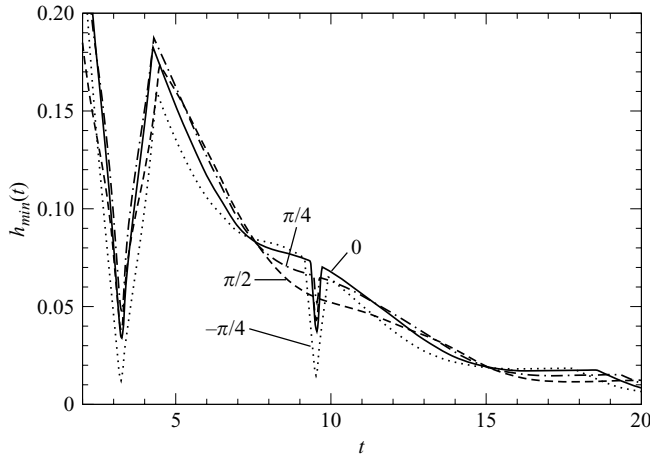


FIGURE 14. Minimum film thickness as a function of time over several cycles with $\lambda = 0.25$, $S = 2 \times 10^{-5}$, $\beta = 10^{-2}$, $V_0 = 1.576$, $Q_{mT} = 0.02$ and $Q_{OT} = 0.08$; the additional phase shifts ψ are noted by the curves.

λ to maintain periodic behaviour; the narrower gap at the closed state is needed to offset the net drainage that occurs at the right-hand boundary. Table 1 shows the approximate boundary between periodic behaviour for different boundary fluxes. As the flux through the boundaries increases, the gap width at the closed state must decrease to maintain periodic behaviour of the film. The case with smaller initial volume appears to be more sensitive to the boundary fluxes.

Finally, we study the phase dependence of the inflow and outflow at the ends by using non-zero ψ in (2.21). We choose $\psi = -\pi/4, \pi/4, \pi/2$ and compare to our case of $\psi = 0$ considered above. The top and bottom fluxes are kept in phase to remain consistent with the tear film drainage problem in the eye. The dependence on ψ is complicated but not dramatic; figure 14 shows the evolution of the minimum film thickness over the blink cycle for the case with $\lambda = 0.25$, $S = 2 \times 10^{-5}$, $V_0 = 1.576$, $Q_{mT} = 0.02$ and $Q_{OT} = 0.08$. This case was chosen because it showed a relatively large effect; the curves with the positive ψ show an increased minimum for the fully open film, while $\psi = -\pi/4$ shows a decreased minimum thickness. Other than these changes in the minimum, the differences in $h(x, t)$ are relatively small and these results are omitted.

3.3. Large- M limit

The uniform-stretching, or large- M , limit yields similar results with some new features. In figure 15, we show a time sequence of the case with $\lambda = 0.5$ and $S = 2 \times 10^{-5}$. The same qualitative shape is retained once the domain has fully opened; the plateau in the right half, in the main, expands and contracts as the domain length changes. This is in contrast to the stress-free case where a film is laid down and then taken up in a nearly reversible manner (as in figure 11, for example). In the partial blink results of figure 15, the left end shows capillary-driven thinning, which is similar to the stress-free case.

Another partial blink approximation would be to start the computation in a more closed state, allow the domain to open, and then start half-blinks; this would correspond to using a small value, say $\lambda = \lambda_0$, in (2.17) for the first half-cycle, then using a larger λ for any remaining lid motion. Results for starting at $\lambda_0 = 0.25$,

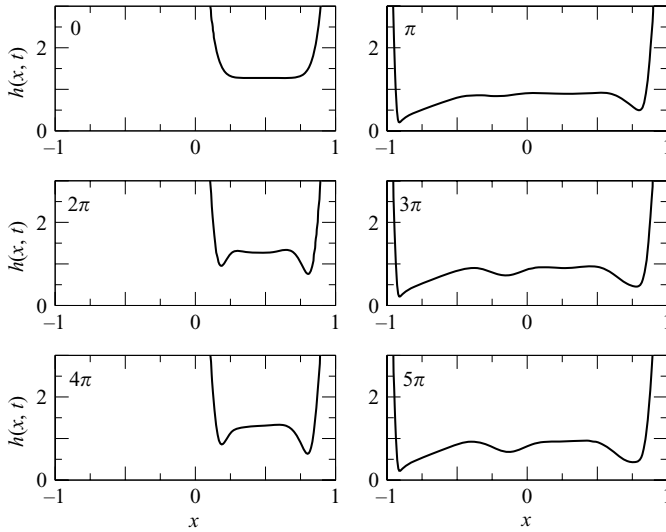


FIGURE 15. A series of half-blinks starting from the half-closed position ($\lambda = 0.5$). $S = 2 \times 10^{-5}$, $m = 8$, $Q_{mT} = Q_{0T} = 0$, $V_0 = 2.576$. The effect of uniform stretching is apparent.

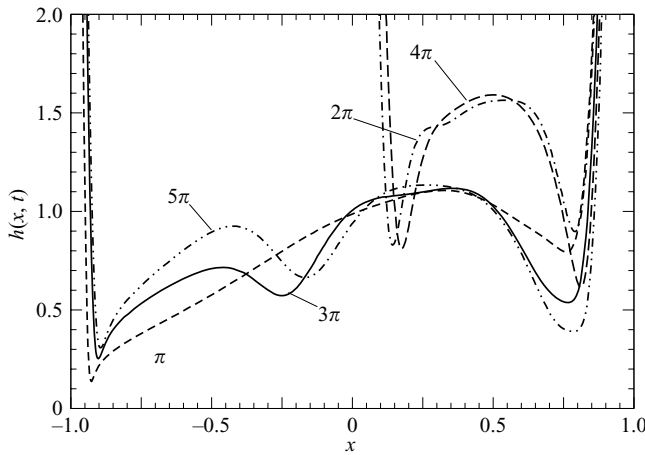


FIGURE 16. A series of half-blinks opening from $\lambda_0 = 0.25$ and then repeated closing to $\lambda = 0.5$ with fluxes through the boundary. $S = 2 \times 10^{-5}$, $Q_{mT} = 0.02$, $Q_{0T} = 0.04$, $m = 8$, $V_0 = 2.576$. The minimum thickness of the initial condition is too high to be seen.

opening fully and then repeatedly closing to $\lambda = 0.5$ are shown in figure 16. We see that the fully open film profiles (odd multiples of π) have a roughly flat region in the right half with a dip in the centre and a decreasing film thickness on the left. The film shapes at $t = 3\pi$ and 5π compare well with our qualitative interpretation of the *in vivo* image to be discussed in § 4.

A comparison of the three cases at $t = \pi$ is shown in figure 17; the uniform-stretching result is more uniform in thickness than the stress-free result for the same initial condition in all cases. Figure 17(a) shows results for $V_0 = 2.576$ and $m = 8$. For $V_0 = 1.576$, figure 17(b) shows results for $m = 16$ and figure 17(c) for $m = 8$. The reduced variation in thickness for the uniform-stretching case is more easily

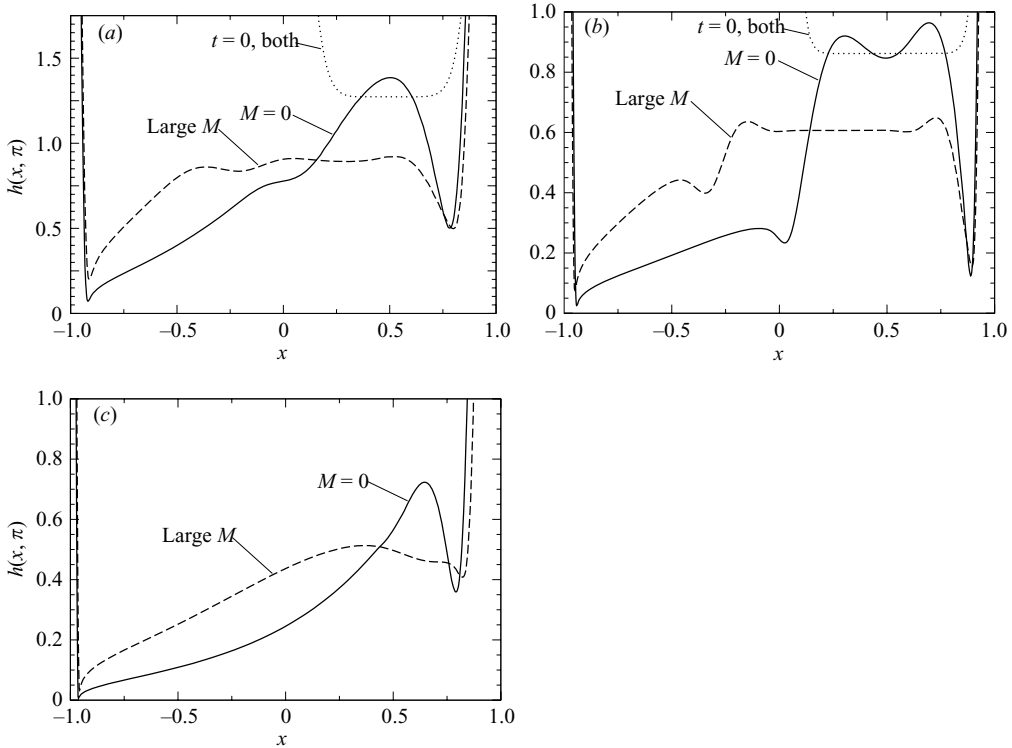


FIGURE 17. Comparisons of the stress-free ($M = 0$) and the uniform-stretching limit ($M \gg 1$) at $t = \pi$. Initial condition using (a) $\lambda = 0.5$, $m = 8$ and $V_0 = 2.576$; (b) $\lambda = 0.5$, $m = 16$ and $V_0 = 1.576$; (c) $\lambda = 0.1$, $m = 8$ and $V_0 = 1.576$.

seen for larger m and smaller V_0 or for larger V_0 and smaller m . Figure 17(b) has a more pronounced flat region in the right-hand side of the film for either case; this plateau-type region survived longer for $V_0 = 1.576$ because the thinner film slows down the capillary-driven smoothing of this part of the film. Figure 17(a) does not have a separate plateau region, but it does show a film from a partial blink that attains a good level of uniformity without having an influx through the moving end. Thus it may not be uniformly true that a flux through the lids is always needed to produce a sound tear film.

Finally, the amount of closure required to obtain a periodic solution is shown in table 2; it is more than in the stress-free model, that is, less of the film remains open in order to achieve periodicity in the solution.

3.4. Experimental thickness and comparison with theory

The partial blink modelling in this paper appears to capture some observed behaviour in the tear film, despite its simplicity. After the pioneering work of Doane (1989), King-Smith and coworkers have published a series of papers on measuring the tear film thickness using interferometry (e.g. King-Smith *et al.* 2000; Nichols & King-Smith 2003; King-Smith *et al.* 2004, 2006). The clearest images come from the pre-lens tear film (PLTF) because the best contrast between tear fluid and the underlying surface occurs in that case; we use a result from a PLTF for comparison with our simulations for this reason. A half-blink was captured on film and it showed a distinctive fringe

Q_{mT}	Q_{0T}	λ	
		$V_0 = 1.576$	$V_0 = 2.576$
0	0	0.157	0.193
0.01	0.02	0.136	0.189
0.02	0.04	0.131	0.186
0.04	0.08	0.127	0.184

TABLE 2. The beginning of non-periodic behaviour is estimated for the given values of λ at various boundary flux conditions with $S = 2 \times 10^{-5}$ and $h_0 = 13$. These results are for the $M \gg 1$ or uniform stretching case. We believe that these estimates are accurate to within ± 0.002 .

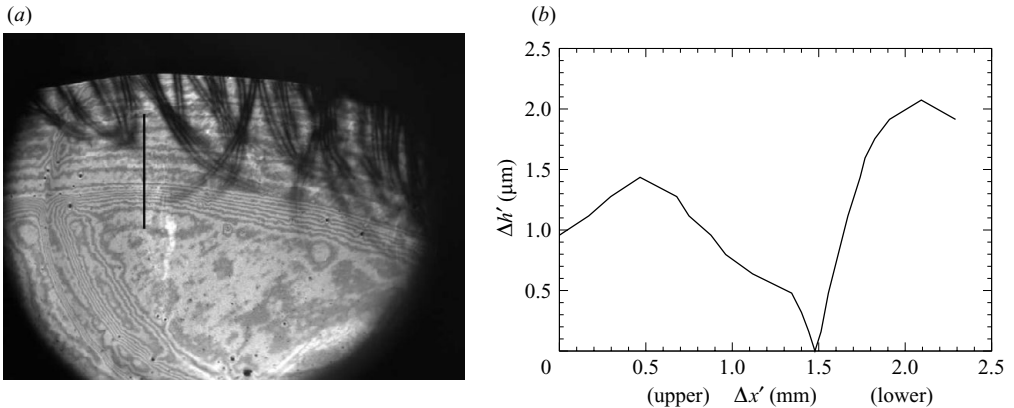


FIGURE 18. (a) Interference fringes for the total tear film thickness of the PLTF just after a half-blink. The horizontal extent of the image is about 8 mm; the thickness difference between neighbouring bright fringes is $0.32 \mu\text{m}$. The upper lid descended to the region of compact fringes in the middle of the image and then rose to the open position (upper lashes still visible). The curving feature near the left-hand edge of the illuminated region is the edge of the optic zone of the lens (see text). (b) Dimensional thickness variation relative to the minimum found was computed from the image along the vertical line in the upper left quadrant. Comparison of broad and narrow band contrast leads to an estimated minimum film thickness of $0.48 \mu\text{m}$. This thickness variation compares qualitatively with a number of results in this paper.

pattern; Doane (1980) has pointed out that partial blinks are not uncommon, which makes this a relevant case for comparison. An image of the PLTF just after a half-blink is shown in figure 18. The interference fringes shown in the photo are consistent with the computations in this paper, within the limits of the theory. This can be seen as follows. Thickness variation was computed from the image in figure 18(a) using the interference fringes; the variation along the vertical line is shown in figure 18(b). Near the bottom end of this line, there is a rather flat region (in the lower half of the figure). Moving up, a rapid decrease in film thickness is encountered about the middle of the photo, and then an increase in thickness occurs. Finally, in the uppermost part of the figure, the film thickness decreases once again. We note that the ends of the film (in particular the menisci and neighbouring regions) are not included in that comparison because they are not captured in the interference fringe image. Note also that the variation in space of the film thickness is very gradual because of the difference in scales for the axes in figure 18(b).

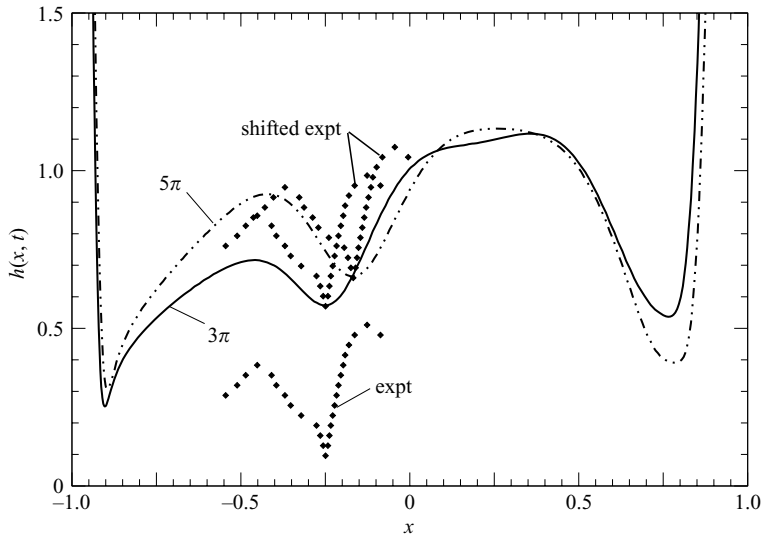


FIGURE 19. Comparison of tear film thickness variation from the interference patterns and the computed results for the uniform-stretching limit. For the computed results, the ends of the film started at $\lambda_0 = 0.25$ and then repeatedly closed to $\lambda = 0.5$ with non-zero fluxes through the ends, $Q_{mT} = 0.02$, $Q_{0T} = 0.04$, $m = 8$, $v = 2.576$. The symbols labelled 'expt' used an estimated minimum tear film thickness of $0.48 \mu\text{m}$; the symbols labelled 'shifted expt' have been shifted to have coincident minima with the computed curves.

In order to compare with computed results, this thickness variation from experiment was non-dimensionalized and shifted so that the minimum film thickness from measurements coincided with those of the computed results in order to facilitate comparison. The results are shown in figure 19, with the symbols corresponding to experimental results. The comparison is qualitative, and seems to be better for the $t = 5\pi$ curve; this appears to be a relatively good comparison given the simplified motion of the ends of the film compared to real blink motions. Trying to make still closer comparisons for these computed results does not seem appropriate at this point given the simplifications used in the modelling; we believe that more realistic lid motion functions and fluxes are required for this purpose. Representative efforts to obtain the overall thickness closer to the experimental observation is shown in figure 20; the computed results are shown at $t = 3\pi$ for various initial conditions. In that figure, the overall thickness of the film is in better agreement, but the details of the valley do not match as well. In particular, for smaller volumes, the computed shape is better for the average thickness and the local minimum in the middle. For larger initial volumes, the depth of the valley in the middle of the film is better, but the average thickness of the film is too large by about a factor of 3 for the cases shown.

The curving feature near the left-hand edge of the illuminated region of figure 18 is the edge of the optic zone of the lens. There is a change in slope at the edge of the optic zone (typically a 3 mm radius) where the shape of the lens changes from optical requirements for improved vision to mechanical requirements for comfort and durability (outside radius of 6 or 7 mm). In this case, the fringes are consistent with a rapid change in the tear film thickness at the edge of the optic zone.

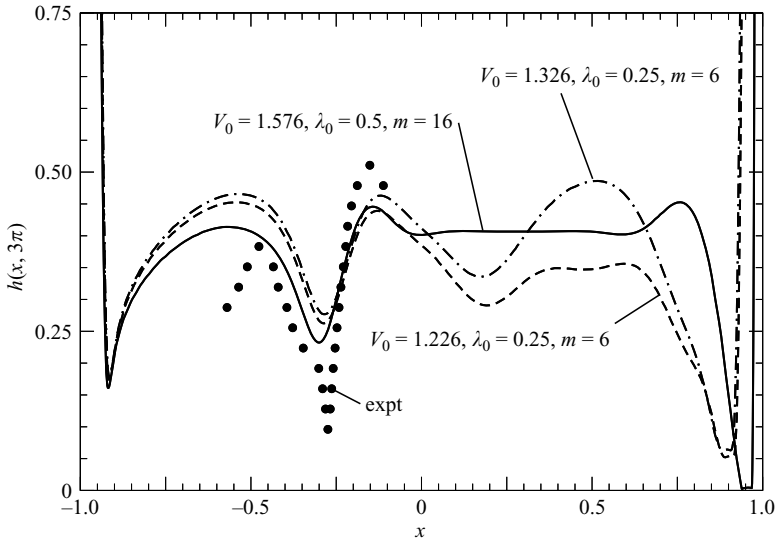


FIGURE 20. Comparison of tear film thickness variation from the interference patterns and the computed results in the uniform-stretching case at $t = 3\pi$ (apparently the optimal time for comparison) and $s = 2 \times 10^{-5}$, $Q_{mT} = 0.02$, $Q_{0T} = 0.04$. For the computed results, the ends of the film started at various λ_0 , V_0 and m and then repeatedly closed to $\lambda = 0.5$ with non-zero fluxes through the ends.

4. Discussion

Our results confirm the conclusion of Jones *et al.* (2005) that the film would rupture before coating the whole substrate without influx from the moving end for opening after a complete blink, if van der Waals type forces were present to drive rupture. This conclusion is reached because in the cases without influx ($Q_{mT} = Q_{0T} = 0$), the minimum film thickness is significantly lower than 100 nm dimensionally at the fully open state, and such small thicknesses would be vulnerable to rupture in the presence of suitable van der Waals forces. In fact, a number of cases that included influx from the moving end may still be prone to rupture because the minimum thickness was increased, but typically not enough to avoid the submicron range when the film reached the fully open state.

However, we note that figure 17(a) had a particularly uniform film shape that arose from a partial blink in the uniform-stretching model with no-flux boundary conditions at the lid. This was not seen in simulations that began from a fully closed state in the work of Jones *et al.* (2005). They concluded that a tear film could not be formed without an influx of tears from under the lids; this statement is true for opening following a complete closure, but it is not true for a half-blink for at least some models and initial conditions. One must be specific about the conditions when flux is needed to form a film; we intend to investigate this further in future work.

Adding flux into and out of the film using sinusoidal functions does show that the minimum film thickness is increased, but for partial blinks, the extraction of fluid from the stationary end can shorten the life of the film, while increasing the thickness in the swept portion of the film. If the swept portion is large enough, then the film thickness appears to be a periodic function according to our numerical results. This happens because the film is swept up enough to erase any prior evidence of local minima at either end of the film; this may be a possible explanation as to why

many blinks do not have the lids completely closed (Doane 1980). The amount of swept portion that is required to achieve periodic behaviour depends mildly on the flux conditions at the ends; the larger the flux, the more closed the eye must be to achieve periodic behaviour. In our model problems, this is because only efflux of tear fluid occurs at the stationary end corresponding to the bottom lid and so the influx from the moving end must move near enough to supply new fluid to the stationary end.

When the eye does not ‘fully close’ enough to cause periodic behaviour, we consider the blink to be ‘partial’ and the film behaviour has a swept part that is approximately periodic and an unswept part that is driven by the capillary forces which dominate in drainage flow after a blink (Braun & Fitt 2003; Wong *et al.* 1996; Sharma *et al.* 1998; Miller *et al.* 2003; McDonald & Brubaker 1971). In the absence of any flux through the stationary end of the film, there is a slow decay of the minimum film thickness driven only by capillarity. When a non-zero flux leaving the film is added to the stationary end, the decrease in h is accelerated and a series of partial blinks in this case leads to rupture of the film near that end. Thus, in these models, depending on the conditions, rupture may occur near either end of the film. While tear film breakup (rupture) in eyes may often occur away from the film edges (Bitton & Lovasik 1998), there is experimental evidence for breakup near the edges (see e.g. McDonald & Brubaker 1971; King-Smith *et al.* 2005).

We do note that similar thickness profiles occur in the corresponding region of the computed figures 8(a), 10, 16 and 17; to a lesser extent similar profiles are seen in figure 15. Weaker comparison with measured tear film thicknesses may be seen in figures 15 and 17(a) because they do not have a deep enough dip in the middle of the film where the lid would have stopped at $t = 3\pi$, but figure 15 is the better of the two in this respect. For many of the stress-free cases, the computed film shapes are less likely to have a plateau-like region in the right half of a plot corresponding to the lower part of the fringe pattern. What is perhaps most encouraging is that, for the uniform-stretching case in particular, similar film shapes arise from several reasonable computations, and so the result may be robust. Jones *et al.* (2006) computed film profiles with valleys in the middle of the film from partial blinks that were not complete blink cycles for a model with mobile free surface and surfactant transport as well.

The maximum amount of open eye during the blink that still allowed periodic film evolution was determined empirically from the computations. This was interpreted as the range of values that had the same functional effect as a complete closure of the lids with respect to resetting the tear film after the blink. Knowing these values may suggest useful values in clinical settings for what range of blinks works as effectively as completely closed lids for the purpose of regenerating the tear film.

5. Conclusion

Despite the simplified nature of our model problems, there are some encouraging comparisons that may be made with observations of the tear film. First, multiple blink cycles were computed. These blink cycle models have given some insight into when a blink is effectively behaving as a complete one, using periodicity as a test of the effectiveness of a blink. Differences between the limiting cases of stress-free and uniformly-stretching surfaces were found, and the stretching of film shapes in the latter case could certainly be observed. The models also gave qualitative agreement with observed tear film thickness profiles measured *in vivo* following a half-blink.

In this paper, we developed a theoretical foundation for the blink cycle assuming sinusoidal lid motion and boundary flux functions. While this is a beginning, it is important to implement the models with realistic lid motion functions (Jones *et al.* 2005; Doane 1980; Berke & Mueller 1996, 1998); results for that case are in hand (Heryudono *et al.* 2007). Additional extensions underway are a model with a mobile free surface and surfactant transport. We believe that these new ingredients will continue to bring new insights into tear film formation and drainage.

R.J.B. thanks L.P. Cook and M.G. Doane for helpful discussions and the IMA at the University of Minnesota for its hospitality during parts of this work. P.E.K.S. thanks J.J. and K.K. Nichols, B.A. Fink and R.M. Hill for their advice and assistance. This work was supported in part by NSF grant DMS-0616483.

Appendix. Fixed domain and initial conditions

In order to solve these problems numerically, we map them to a fixed domain using the tranformation (2.22). For the stress-free case mapping onto the fixed domain results in

$$H_t - \frac{1-\xi}{L-X} X_t H_\xi + \left(\frac{2}{L-X}\right) \left\{ \left(\frac{H^3}{3} + \beta H^2\right) \left[\left(\frac{2}{L-X}\right)^3 S H_{\xi\xi\xi} + G \right] \right\}_\xi = 0.$$

This equation is subject to the boundary conditions

$$H(\pm 1, t) = h_0$$

at each end. At the lower lid ($\xi = 1$), also

$$\left(\frac{h_0^3}{3} + \beta h_0^2\right) \left[\left(\frac{2}{L-X}\right)^3 S H_{\xi\xi\xi}(1, t) + G \right] = -Q_{bot};$$

this is the standard flux condition at the stationary wall. At the upper lid ($\xi = -1$),

$$\left(\frac{h_0^3}{3} + \beta h_0^2\right) \left[\left(\frac{2}{L-X}\right)^3 S H_{\xi\xi\xi}(-1, t) + G \right] = X_t h_0 + Q_{top};$$

the first term on the right-hand side comes from the volume swept out by the upper lid, while the left-hand side eliminates that same volume when the imposed flux Q_{top} is zero. Note that Q_{bot} and Q_{top} are the fluxes into the domain.

For the uniform-stretching case

$$H_t - X_t \frac{2}{L-X} \frac{1-\xi}{2} H_\xi + X_t \frac{2}{L-X} \left[\frac{1-\xi}{2} \frac{H}{2} \left(1 + \frac{\beta}{H+\beta} \right) \right]_\xi + \frac{2}{L-X} \left\{ \frac{H^3}{12} \left(1 + \frac{3\beta}{H+\beta} \right) \left[S \left(\frac{2}{L-X}\right)^3 H_{\xi\xi\xi} + G \right] \right\}_\xi = 0$$

The boundary conditions are in this case are as follows. The ends are still pinned at $H(\pm 1, t) = h_0$. At the lower lid ($\xi = 1$),

$$X_t \frac{h_0}{2} \left(1 + \frac{\beta}{h_0 + \beta} \right) + \frac{h_0^3}{12} \left(1 + \frac{3\beta}{h_0 + \beta} \right) \left[S \left(\frac{2}{L-X}\right)^3 H_{\xi\xi\xi} + G \right] = -Q_{bot}$$

for a specified volume flux Q_{bot} through this end. At the upper lid ($\xi = -1$),

$$X_t \frac{h_0}{2} \left(1 + \frac{\beta}{h_0 + \beta} \right) + \frac{h_0^3}{12} \left(1 + \frac{3\beta}{h_0 + \beta} \right) \left[S \left(\frac{2}{L - X} \right)^3 H_{\xi\xi\xi} + G \right] = X_t h_0 + Q_{top}.$$

REFERENCES

- BERGER, R. E. & CORRISIN, S. 1974 A surface tension gradient mechanism for driving the pre-corneal tear film after a blink. *J. Biomech.* **7**, 225–238.
- BERIS, A., ARMSTRONG, R. C. & BROWN, R. A. 1983 Perturbation theory for viscoelastic fluids between eccentric rotating cylinders. *J. Non-Newtonian Fluid Mech.* **13**, 109–148.
- BERKE, A. & MUELLER, S. 1996 Einfluss des lidschlages auf die kontaktlinse und die zugrundeliegenden kräfte. *Die Kontaktlinse* **1**, 17–26.
- BERKE, A. & MUELLER, S. 1998 The kinetics of lid motion and its effects on the tear film. In *Lacrimal Gland, Tear Film, and Dry Eye Syndromes 2* (ed. D. A. Sullivan, D. A. Dartt & M. A. Meneray), pp. 417–424. Plenum.
- BITTON, E. & LOVASIK, J. V. 1998 Longitudinal analysis of precorneal tear film rupture patterns. In *Lacrimal Gland, Tear Film and Dry Eye Syndromes 2* (ed. D. A. Sullivan, D. A. Dartt & M. A. Meneray), pp. 381–389. Plenum.
- BRAUN, R. J. 2006 Models for human tear film dynamics. In *Wave Dynamics and Thin Film Flow Systems* (ed. R. Usha, A. Sharma & B. S. Dandapat), pp. 404–434. Narosa.
- BRAUN, R. J. & FITT, A. D. 2003 Modelling drainage of the precorneal tear film after a blink. *Math. Med. Bio.* **20**, 1–28.
- BRENAN, K. E., CAMPBELL, S. L. & PETZOLD, L. R. 1996 *Numerical Solution of Initial-Value Problems in Differential Algebraic Equations*. SIAM.
- BRON, A. J., TIFFANY, J. M., GOUVEIA, S. M., YOKOI, N. & VOON, L. W. 2004 Functional aspects of the tear film lipid layer. *Expl Eye Res.* **78**, 347–360.
- CHEN, H.-B., YAMABAYASHI, S., OU, B., TANAKA, Y. & OHNO, S. 1997 Structure and composition of rat precorneal tear film: A study by in vivo cryofixation. *Invest. Ophthalmol. Vis. Sci.* **38**, 381–387.
- CREECH, J. L., DO, L. T., FATT, I. & RADKE, C. J. 1998 In vivo tear-film thickness determination and implications for tear-film stability. *Curr. Eye Res.* **17**, 1058–1066.
- DOANE, M. G. 1980 Interaction of eyelids and tears in corneal wetting and the dynamics of the normal human eyeblink. *Am. J. Ophthalmol.* **89**, 507–516.
- DOANE, M. G. 1981 Blinking and the mechanics of the lacrimal drainage system. *Ophthalmol.* **88**, 844–51.
- DOANE, M. G. 1989 An instrument for in vivo tear film interferometry. *Optom. Vis. Sci.* **66**, 383–388.
- EHLERS, N. 1965 The precorneal film: Biomicroscopical, histological and chemical investigations. *Acta Ophthalmol. Suppl.* **81**, 3–135.
- FATT, I. & WEISSMAN, B. A. 1992 *Physiology of the Eye – An introduction to the Vegetative Functions*, 2nd edn. Butterworth-Heinemann.
- FOGT, N., KING-SMITH, P. E. & TUELL, G. 1998 Interferometric measurement of tear film thickness by use of spectral oscillations. *J. Opt. Soc. Am. A* **15**, 268–275.
- GIPSON, I. K. 2004 Distribution of mucins at the ocular surface. *Expl Eye Res.* **78**, 379–388.
- HERYUDONO, A., BRAUN, R. J., DRISCOLL, T. A., COOK, L. P. & KING-SMITH, P. E. 2007 Single-equation models for the tear film in a blink cycle: Realistic lid motion. Submitted.
- HUH, C. & SCRIVEN, L. E. 1971 Hydrodynamic model of a steady movement of a solid/liquid/fluid contact line. *J. Colloid Interface Sci.* **35**, 85–101.
- JONES, M. B., MCELWAIN, D. L. S., FULFORD, G. R., COLLINS, M. J. & ROBERTS, A. P. 2006 The effect of the lipid layer on tear film behavior. *Bull. Math. Bio.* **68**, 1355–1381.
- JONES, M. B., PLEASE, C. P., MCELWAIN, D. L. S., FULFORD, G. R., ROBERTS, A. P. & COLLINS, M. J. 2005 Dynamics of tear film deposition and draining. *Math. Med. Bio.* **22**, 265–288.
- KING-SMITH, P. E., FINK, B. A., FOGT, N., NICHOLS, K. K., HILL, R. M. & WILSON, G. S. 2000 The thickness of the human precorneal tear film: Evidence from reflection spectra. *Invest. Ophthalmol. Vis. Sci.* **41**, 3348–3359.

- KING-SMITH, P. E., FINK, B. A., HILL, R. M., KOELLING, K. W. & TIFFANY, J. M. 2004 The thickness of the tear film. *Curr. Eye Res.* **29**, 357–368.
- KING-SMITH, P. E., FINK, B. A., HILL, R. M., KOELLING, K. W. & TIFFANY, J. M. 2005 Reply to letter by Dr. C. J. Radke. *Curr. Eye Res.* **30**, 1133–1134.
- KING-SMITH, P. E., FINK, B. A., NICHOLS, J. J., NICHOLS, K. K. & HILL, R. M. 2006 The thickness of the human precorneal tear film: Evidence from reflection spectra. *J. Opt. Soc. Am. A* **23**, 2097–2104.
- KORB, D. R. & HERMAN, J. P. 1979 Corneal staining subsequent to sequential fluorescein instillations. *J. Am. Optom. Assoc.* **50**, 361–367.
- LEE, A. G., SHAQFEH, E. S. G. & KHOMAMI, B. 2002 A study of viscoelastic free surface flows by the finite element method: Hele-shaw and slot coating flows. *J. Non-Newtonian Fluid Mech.* **108**, 327–362.
- LEVICH, V. G. 1962 *Physicochemical Hydrodynamics*. Wiley.
- MCCULLEY, J. P. & SHINE, W. 1997 A compositional based model for the tear film lipid layer. *Trans. Am. Ophthalm. Soc.* **XCIV**, 79–93.
- MCDONALD, J. E. & BRUBAKER, S. 1971 Meniscus-induced thinning of tear films. *Am. J. Ophthalmol.* **72**, 139–146.
- MILLER, K. L., POLSE, K. A. & RADKE, C. J. 2003 On the formation of the black line. *Curr. Eye Res.* **25**, 155–162.
- MISHIMA, S. 1965 Some physiological aspects of the precorneal tear film. *Arch. Ophthalmol.* **73**, 233–241.
- MYERS, T. G. 2005 Application of non-Newtonian models to thin film flow. *Phys. Rev. E* **72**, 066302.
- NICHOLS, J. J. & KING-SMITH, P. E. 2003 Thickness of the pre- and post-contact lens tear film measured in vivo by interferometry. *Invest. Ophthalmol. Vis. Sci.* **44**, 68–77.
- ORON, A., DAVIS, S. H. & BANKOFF, S. G. 1997 Long-scale evolution of thin liquid films. *Rev. Mod. Phys.* **69**, 931–980.
- OWENS, H. & PHILLIPS, J. 2001 Spread of the tears after a blink: Velocity and stabilization time in healthy eyes. *Cornea* **20**, 484–487.
- PANDIT, J. C., NAGYOVÁ, B., BRON, A. J. & TIFFANY, J. M. 1999 Physical properties of stimulated and unstimulated tears. *Expl Eye Res.* **68**, 247–253.
- PASQUALI, M. & SCRIVEN, L. E. 2002 Free surface flows of polymer solutions with models based on the conformation tensor. *J. Non-Newtonian Fluid Mech.* **108**, 363–409.
- PROBSTEIN, R. F. 1994 *Physicochemical Hydrodynamics*. Wiley.
- ROLANDO, M. & REFOJO, M. F. 1983 Tear evaporimeter for measuring water evaporation rate from the tear film under controlled conditions in humans. *Expl Eye Res.* **36**, 25–33.
- SHARMA, A., KHANNA, R. & REITER, G. 1999 A thin film analog of the corneal mucus layer of the tear film: an enigmatic long range non-classical dlvo interaction in the breakup of thin polymer films. *Colloids Surf. B* **14**, 223–235.
- SHARMA, A., TIWARI, S., KHANNA, R. & TIFFANY, J. M. 1998 Hydrodynamics of meniscus-induced thinning of the tear film. In *Lacrimal Gland, Tear Film, and Dry Eye Syndromes 2* (ed. D. A. Sullivan, D. A. Dartt & M. A. Meneray), pp. 425–431. Plenum.
- TIFFANY, J. M. 1991 The viscosity of human tears. *Intl Ophthalmol.* **15**, 371–376.
- TIFFANY, J. M. 1994 Viscoelastic properties of human tears and polymer solutions. In *Lacrimal Gland, Tear Film, and Dry Eye Syndromes* (ed. D. A. Sullivan), pp. 267–270. Plenum.
- WANG, J., FONN, D., SIMPSON, T. L. & JONES, L. 2003 Precorneal and pre- and postlens tear film thickness measured indirectly with optical coherence tomography. *Invest. Ophthalmol. Vis. Sci.* **44**, 2524–2528.
- WONG, H., FATT, I. & RADKE, C. J. 1996 Deposition and thinning of the human tear film. *J. Colloid Interface Sci.* **184**, 44–51.
- ZHANG, L., MATAR, O. K. & CRASTER, R. 2003a Analysis of tear film rupture: Effect of non-Newtonian rheology. *J. Colloid Interface Sci.* **262**, 130–148.
- ZHANG, L., MATAR, O. K. & CRASTER, R. 2003b Surfactant driven flows overlying a hydrophobic epithelium: film rupture in the presence of slip. *J. Colloid Interface Sci.* **264**, 160–175.
- ZHANG, R. & LI, X. K. 2005 Non-Newtonian effects on lubricant thin film flows. *J. Engng Maths* **51**, 1–13.